PHYSICAL REVIEW D **84,** 114023 (2011)

Contribution of higher nucleon resonances to $K^*\Lambda$ photoproduction

Sang-Ho Kim,[1,*] Seung-il Nam,[2,†] Yongseok Oh,[3,2,‡] and Hyun-Chul Kim[1,2,§]

[1]*Department of Physics, Inha University, Incheon 402-751, Korea*
[2]*School of Physics, Korea Institute for Advanced Study, Seoul 130-722, Korea*
[3]*Department of Physics, Kyungpook National University, Daegu 702-701, Korea*

(Received 29 October 2011; published 19 December 2011)

We investigate $K^*\Lambda(1116)$ photoproduction off the proton and neutron targets using the effective Lagrangian method in the tree-level Born approximation. In addition to the K, K^*, and κ exchanges which are the main contributions to the reaction, we consider the contributions from the higher nucleon resonances $D_{13}(2080)$ and the $D_{15}(2200)$. We find that the $D_{13}(2080)$ plays a crucial role in explaining the enhancement of the near-threshold production rate, which results in a good agreement with the experimental data for the proton targets, while the contribution of the $D_{15}(2200)$ is rather small. A similar conclusion is drawn for K^* photoproduction off the neutron targets. In addition to the energy and angular dependence of the cross sections, we present the predictions on the photon-beam asymmetry.

DOI: 10.1103/PhysRevD.84.114023 PACS numbers: 13.60.Le, 14.20.Gk

I. INTRODUCTION

Strange meson and baryon photoproductions provide a very useful tool in studying the properties of strange hadrons and, in particular, in examining the structure of nonstrange baryon resonances that cannot be seen in the nonstrange πN channel. This was shown manifestly in the investigation of kaon photoproduction off the nucleon targets, i.e., $\gamma N \to K\Lambda(1116)$, which has been studied intensively both theoretically and experimentally [1–9]. These works show that nucleon resonances play a crucial role in understanding the production mechanisms of the reaction in the resonance region [6,7].

The recent upgrade plans of the photon-beam facilities such as the LEPS2 project at SPring-8 [10] and the CLAS12 project at Thomas Jefferson National Accelerator Facility (TJNAF) [11] will enable us to study the photoproduction processes of heavier strange mesons with an unprecedented accuracy. This will enrich our understanding of strange hadrons. In particular, the production of strange vector mesons can be investigated in detail. The experimental studies on the exclusive production of the K^* vector mesons from photon-nucleon scattering have been reported only recently [12–14].[1] These experiments have measured mostly the total and the differential cross sections and have shown that although the cross sections of K^* photoproduction are small compared to those of kaon photoproduction, their values are nonnegligible. It indicates that production reactions with heavier strange hadrons should be considered when analyzing higher nucleon resonances, which are still less known theoretically as well as experimentally (see, for example, the Particle Data Group (PDG) compilation for the N^* resonances [15]). We expect that the upgrades of the experimental facilities can offer a chance to study various physical quantities of K^* photoproduction in detail so that one can have enough data for unraveling the excited spectra of the nonstrange baryon resonances. Theoretically, K^* photoproduction was studied in a quark model [16] and in the effective Lagrangian approach [17,18]. In particular, Refs. [17,18] have emphasized the role of the t-channel scalar κ meson exchange and have suggested its experimental test.

Recently, new experimental data were announced by the CLAS Collaboration at TJNAF [3,19] for the angular distribution of the cross sections for the reaction of $\gamma p \to K^{*+}\Lambda$. When compared with previous theoretical calculations [17,18,20], the new data show that the prediction of the model of Refs. [17,18] underestimates the cross sections near the threshold, which is in the N^* resonance region. Therefore, it is legitimate to reconsider the theoretical model of Refs. [17,18] with higher nucleon resonances being taken into account.

In the present paper, we investigate $K^*\Lambda$ photoproduction off the nucleon targets, i.e., $\gamma p \to K^{*+}\Lambda$ and $\gamma n \to K^{*0}\Lambda$. Employing the effective Lagrangian method in the tree-level Born approximation, we improve the model of Refs. [17,18] by including the contributions of nucleon resonances. Because of isospin conservation, intermediate Δ resonances are not allowed and nucleon resonances can only contribute to this process. Therefore, it is of great significance to extract carefully parameters of the N^* resonances such as their coupling strengths to the K^* and the $\Lambda(1116)$. More reliable resonance parameters might be obtained by full partial-wave analyses. However, since the threshold energy of $K^*\Lambda$ production is about 2 GeV, it is reasonable to start with only the $N(2080, 3/2^-)$ and the

*sanghokim@ihha.edu
†sinam@kias.re.kr
‡yohphy@knu.ac.kr
§hchkim@inha.ac.kr

[1]The numerical error of a factor of 3/2 in the data reported in Refs. [12,13] was pointed out in Ref. [14] and was corrected later. See Ref. [13].

$N(2200, 5/2^-)$ as relevant nucleon resonances for this process near the threshold.[2] We will show that these two resonances, $N(2080, 3/2^-)$ and $N(2200, 5/2^-)$, are enough to address the important role of nucleon resonances in this reaction. Following the model of Ref. [18], we also take into account other production mechanisms that include the nucleon (N) and hyperon (Λ, Σ, Σ^*) pole contributions in the s and u channels, respectively, and the exchanges of strange mesons (κ, K, K^*) in the t channel. A contact-term contribution is considered as well in order to fulfill the current conservation of the electromagnetic interactions.

This paper is organized as follows. In Sec. II, we briefly introduce the framework of our model. The effective Lagrangians for the resonance interactions are given explicitly as well as those for the background production mechanisms. All the parameters used in the present calculation are given explicitly. We compare our results of the cross sections with the experimental data for the reaction of $\gamma p \to K^*\Lambda$ in Sect. III. The predictions on the photon-beam asymmetries are then discussed. We also discuss the dependence of these physical quantities on isospin. Section IV summarizes and draws conclusions.

II. FORMALISM

In the present work, we employ the effective Lagrangian method at the tree-level Born approximation. The relevant Feynman diagrams for the reaction mechanisms of $\gamma N \to K^*\Lambda$ are shown in Fig. 1, which include the nucleon and nucleon resonance poles in the s channel, the K^*, K, and κ meson exchanges in the t channel, and Λ, Σ, and $\Sigma^*(1385, 3/2^+)$ hyperon terms in the u channel. The contact term is also taken into account to preserve the gauge invariance.

The effective Lagrangians for the background production mechanisms are essentially the same as those used in Refs. [17,18]. As for the photon interaction Lagrangians of strange mesons, we have

$$\begin{aligned}
\mathcal{L}_{\gamma K^*K^*} &= -ie_{K^*}A^\mu(K^{*\nu}K^{*\dagger}_{\mu\nu} - K^*_{\mu\nu}K^{*\dagger\nu}),\\
\mathcal{L}_{\gamma K^*K} &= g_{\gamma KK^*}\varepsilon^{\mu\nu\alpha\beta}(\partial_\mu A_\nu)(\partial_\alpha K^*_\beta)K + \text{H.c.},\\
\mathcal{L}_{\gamma K^*\kappa} &= g_{\gamma K^*\kappa}A^{\mu\nu}\kappa K^*_{\mu\nu} + \text{H.c.},
\end{aligned} \tag{1}$$

where A_μ, K^*_μ, K, and κ denote the photon, the $K^*(892, 1^-)$ vector meson, the $K(495, 0^-)$ pseudoscalar meson, and the $\kappa(800, 0^+)$ scalar meson, respectively,

[2]Including the resonances below the threshold inevitably leads to larger uncertainties because of the lack of experimental and theoretical information on their coupling constants and form factors. We have examined the effects of those resonances with the parameters given by the quark model of Refs. [21,22], and have found that their contributions are negligibly small.

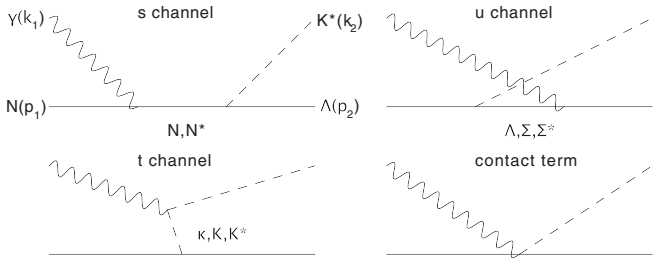

FIG. 1. Feynman diagrams for the $\gamma N \to K^*\Lambda$ reaction.

and $K^*_{\mu\nu} = \partial_\mu K^*_\nu - \partial_\nu K^*_\mu$. The electric charge of the K^* vector meson is denoted by e_{K^*}. We take the values of $g_{\gamma KK^*}$ from the experimental data given by the PDG [15], which leads to $g^{\text{charged}}_{\gamma KK^*} = 0.254\ \text{GeV}^{-1}$ and $g^{\text{neutral}}_{\gamma KK^*} = -0.388\ \text{GeV}^{-1}$, whereas we use the vector-meson dominance [23] to determine the values of $g_{\gamma K^*\kappa}$: $g^{\text{charged}}_{\gamma K^*\kappa} = 0.12e\ \text{GeV}^{-1}$ and $g^{\text{neutral}}_{\gamma K^*\kappa} = -0.24e\ \text{GeV}^{-1}$ with the unit electric charge e.

The Lagrangians for the electromagnetic interactions of baryons are given as

$$\begin{aligned}
\mathcal{L}_{\gamma NN} &= -\bar{N}\left[e_N\not{A} - \frac{e\kappa_N}{2M_N}\sigma_{\mu\nu}\partial^\nu A^\mu\right]N,\\
\mathcal{L}_{\gamma\Lambda\Lambda} &= \frac{e\kappa_\Lambda}{2M_N}\bar{\Lambda}\sigma_{\mu\nu}\partial^\nu A^\mu\Lambda,\\
\mathcal{L}_{\gamma\Lambda\Sigma} &= \frac{e\mu_{\Sigma\Lambda}}{2M_N}\bar{\Sigma}\sigma_{\mu\nu}\partial^\nu A^\mu\Lambda + \text{H.c.},\\
\mathcal{L}_{\gamma\Lambda\Sigma^*} &= -\frac{ie}{2M_N}\left[g^V_{\gamma\Lambda\Sigma^*}\bar{\Lambda}\gamma_\nu - \frac{ig^T_{\gamma\Lambda\Sigma^*}}{2M_N}\partial_\nu\bar{\Lambda}\right]\gamma_5\Sigma^*_\mu F^{\mu\nu}\\
&\quad + \text{H.c.},
\end{aligned} \tag{2}$$

where N, Λ, Σ, and Σ^* stand for the nucleon, $\Lambda(1116)$, $\Sigma(1192)$, and $\Sigma^*(1385, 3/2^+)$ hyperon fields, respectively, and M_h denotes the mass of hadron h. The baryon fields with spin $s \geq 3/2$ are described by the Rarita-Schwinger vector-spinor formalism [24,25]. Here, κ_B is the anomalous magnetic moment of baryon B and $\mu_{\Lambda\Sigma}$ is the transition magnetic moment between the $\Lambda(1116)$ and the $\Sigma(1192)$. Their PDG values are given in Table I. The electromagnetic (EM) coupling with the spin-3/2 hyperon Σ^* has two independent terms as shown in the last line of Eq. (2). These coupling constants are determined by the experimental data for the decay width $\Gamma_{\Sigma^*\to\gamma\Lambda}$ [15], which leads to $(g^V_{\gamma\Lambda\Sigma^*}, g^T_{\gamma\Lambda\Sigma^*}) = (3.78, 3.18)$. The EM couplings in Eqs. (1) and (2) are summarized in Table I.

The effective Lagrangians for the meson-baryon interactions are

TABLE I. Electromagnetic coupling constants for the interactions in Eqs. (1) and (2).

$g^{\text{charged}}_{\gamma K^* K}$	$g^{\text{neutral}}_{\gamma K^* K}$	$g^{\text{charged}}_{\gamma K^* \kappa}$	$g^{\text{neutral}}_{\gamma K^* \kappa}$	κ_n	κ_p	κ_Λ	$\mu_{\Lambda\Sigma}$	$g^V_{\gamma\Lambda\Sigma^*}$	$g^T_{\gamma\Lambda\Sigma^*}$
0.254/GeV	−0.388/GeV	$0.12e$/GeV	$-0.24e$/GeV	1.79	−1.91	−0.61	1.61 ± 0.08	3.78	3.18

$$
\begin{aligned}
\mathcal{L}_{K^*N\Lambda} &= -g_{K^*N\Lambda}\bar{N}\Lambda\left[\not{K}^* - \frac{\kappa_{K^*N\Lambda}}{2M_N}\sigma_{\mu\nu}\partial^\nu K^{*\mu}\right] + \text{H.c.},\\
\mathcal{L}_{K^*N\Sigma} &= -g_{K^*N\Sigma}\bar{N}\Sigma\left[\not{K}^* - \frac{\kappa_{K^*N\Sigma}}{2M_N}\sigma_{\mu\nu}\partial^\nu K^{*\mu}\right] + \text{H.c.},\\
\mathcal{L}_{KN\Lambda} &= -ig_{KN\Lambda}\bar{N}\gamma_5\Lambda K + \text{H.c.},\\
\mathcal{L}_{\kappa N\Lambda} &= -g_{\kappa N\Lambda}\bar{N}\kappa\Lambda + \text{H.c.},\\
\mathcal{L}_{K^*N\Sigma^*} &= -\frac{if^{(1)}_{K^*N\Sigma^*}}{2M_{K^*}}\bar{K}^*_{\mu\nu}\bar{\Sigma}^{*\mu}\gamma^\nu\gamma_5 N - \frac{f^{(2)}_{K^*N\Sigma^*}}{4M^2_{K^*}}\bar{K}^*_{\mu\nu}\bar{\Sigma}^{*\mu}\gamma_5\partial^\nu N + \frac{f^{(3)}_{K^*N\Sigma^*}}{4M^2_{K^*}}\partial^\nu\bar{K}^*_{\mu\nu}\bar{\Sigma}^{*\mu}\gamma_5 N + \text{H.c.},
\end{aligned}
\tag{3}
$$

where $\Sigma = \boldsymbol{\tau}\cdot\boldsymbol{\Sigma}$ and $\Sigma^*_\mu = \boldsymbol{\tau}\cdot\boldsymbol{\Sigma}^*_\mu$. The strong coupling constants can be estimated by the Nijmegen soft-core model (NSC97a) [26], and the corresponding values are presented in Table. II. Considering the minimally possible Lorentz structure for the vector-meson coupling to the Σ^*, we can write the interaction Lagrangian with the three form factors as shown in the last line of Eq. (3), which is similar to the case of $\mathcal{L}_{\gamma\Lambda\Sigma^*}$. From the flavor SU(3) symmetry [27], the value for $f^{(1)}_{K^*N\Sigma^*}$ can be estimated. Because of the lack of experimental and theoretical information on $f^{(2,3)}_{K^*N\Sigma^*}$, we do not consider these terms in the present work, following Ref. [27]. Finally, we have the contact interaction given by

$$
\mathcal{L}_{\gamma K^*N\Lambda} = -\frac{ie_{K^*}g_{K^*N\Lambda}\kappa_{K^*N\Lambda}}{2M_N}\bar{\Lambda}\sigma^{\mu\nu}A_\nu K^*_\mu N + \text{H.c.},
\tag{4}
$$

which is obtained by the minimal gauge substitution $\partial_\mu \to ie_{K^*}A_\mu$ to the $K^*N\Lambda$ interaction.

Considering all the ingredients discussed so far, we obtain the scattering amplitude of each channel as given in Fig. 1:

$$
\begin{aligned}
\mathcal{M}_{t(K^*)} &= \frac{e_{K^*}g_{K^*N\Lambda}}{t-M^2_{K^*}}\varepsilon^*_\nu\bar{u}_\Lambda(2k_2^\mu g^{\nu\alpha} - k_2^\alpha g^{\mu\nu} + k_1^\nu g^{\mu\alpha})\left[g_{\alpha\beta} - \frac{(k_1-k_2)_\alpha(k_1-k_2)_\beta}{M^2_{K^*}}\right]\left[\gamma^\beta - \frac{i\kappa_{K^*N\Lambda}}{2M_N}\sigma^{\beta\delta}(k_1-k_2)_\delta\right]u_N\epsilon_\mu,\\
\mathcal{M}_{t(K)} &= \frac{ig_{\gamma KK^*}g_{KN\Lambda}}{t-M^2_K}\varepsilon^*_\nu\bar{u}_\Lambda\epsilon^{\mu\nu\alpha\beta}k_{1\alpha}k_{2\beta}\gamma_5 u_N\epsilon_\mu,\\
\mathcal{M}_{t(\kappa)} &= -\frac{2g_{\gamma K^*\kappa}g_{\kappa N\Lambda}}{t-(M_\kappa - i\Gamma_\kappa/2)^2}\varepsilon^*_\nu\bar{u}_\Lambda(k_1\cdot k_2 g^{\mu\nu} - k_1^\nu k_2^\mu)u_N\epsilon_\mu,\\
\mathcal{M}_{s(N)} &= \frac{g_{K^*N\Lambda}}{s-M^2_N}\varepsilon^*_\nu\bar{u}_\Lambda\left[\gamma^\nu - \frac{i\kappa_{K^*N\Lambda}}{2M_N}\sigma^{\nu\alpha}k_{2\alpha}\right](\not{k}_1 + \not{p}_1 + M_N)\left[e_N\gamma^\mu + \frac{ie\kappa_N}{2M_N}\sigma^{\mu\beta}k_{1\beta}\right]u_N\epsilon_\mu,\\
\mathcal{M}_{u(\Lambda)} &= \frac{g_{K^*N\Lambda}}{u-M^2_\Lambda}\frac{ie\kappa_\Lambda}{2M_N}\varepsilon^*_\nu\bar{u}_\Lambda\sigma^{\mu\alpha}k_{1\alpha}(\not{p}_1 - \not{k}_2 + M_\Lambda)\left[\gamma^\nu - \frac{i\kappa_{K^*N\Lambda}}{2M_N}\sigma^{\nu\beta}k_{2\beta}\right]u_N\epsilon_\mu,\\
\mathcal{M}_{u(\Sigma)} &= \eta_\Sigma\frac{g_{K^*N\Lambda}}{u-M^2_\Sigma}\frac{ie\mu_{\Sigma\Lambda}}{2M_N}\varepsilon^*_\nu\bar{u}_\Lambda\sigma^{\mu\alpha}k_{1\alpha}(\not{p}_1 - \not{k}_2 + M_\Sigma)\left[\gamma^\nu - \frac{i\kappa_{K^*N\Lambda}}{2M_N}\sigma^{\nu\beta}k_{2\beta}\right]u_N\epsilon_\mu,\\
\mathcal{M}_{u(\Sigma^*)} &= \eta_{\Sigma^*}\frac{f^{(1)}_{K^*N\Sigma^*}}{u-M^2_{\Sigma^*}}\frac{e}{2M_{K^*}}\varepsilon^*_\nu\bar{u}_\Lambda\left[\frac{g_1}{2M_N}\gamma_\sigma + \frac{g_2}{4M_N^2}p_{2\sigma}\right]\gamma_5(k_1^\beta g^{\mu\sigma} - k_1^\sigma g^{\mu\beta})\Delta_{\beta\alpha}\\
&\quad\times(\Sigma^*, p_1-k_2)\gamma_\rho\gamma_5(k_2^\alpha g^{\nu\rho} - k_2^\rho g^{\nu\alpha})u_N\epsilon_\mu,\\
\mathcal{M}_{\text{contact}} &= -\frac{ie_{K^*}g_{K^*N\Lambda}\kappa_{K^*N\Lambda}}{2M_N}\varepsilon^*_\nu\bar{u}_\Lambda\sigma^{\mu\nu}u_N\epsilon_\mu,
\end{aligned}
\tag{5}
$$

TABLE II. Strong coupling constants for the meson-baryon interactions in Eq. (3).

$g_{K^*N\Lambda}$	$\kappa_{K^*N\Lambda}$	$g_{K^*N\Sigma}$	$\kappa_{K^*N\Sigma}$	$\kappa_{KN\Lambda}$	$g_{\kappa N\Lambda}$	$f^{(1)}_{K^*N\Sigma^*}$	$f^{(2)}_{K^*N\Sigma^*}$	$f^{(3)}_{K^*N\Sigma^*}$
−4.26	2.66	−2.46	−0.47	−13.24	−8.3	−5.21	0	0

where ε^*_μ and ϵ_μ indicate the polarization vectors for the outgoing K^* and incoming photon, respectively, and (s, u, t) denote the usual Mandelstam variables. The reaction with the proton (neutron) targets corresponds to η_Σ, $\eta_{\Sigma^*} = +1\,(-1)$. The spin-3/2 Rarita-Schwinger spin projection for the resonance R with momentum p is expressed as

$$\Delta_{\beta\alpha}(R,p) = (\not{p} + M_R)\Big[-g_{\beta\alpha} + \frac{1}{3}\gamma_\beta\gamma_\alpha + \frac{1}{3M_R}(\gamma_\beta p_\alpha - \gamma_\alpha p_\beta) + \frac{2}{3M_R^2}p_\beta p_\alpha\Big]. \quad (6)$$

In addition to the processes discussed above, we now include the nucleon resonance contributions. Here, we consider only the $D_{13}(2080)$ and $D_{15}(2200)$, which lie close to the threshold of K^* photoproduction. Although there are other nucleon resonances near the threshold such as $S_{11}(2090)$ and $P_{11}(2100)$, we have ignored them since they are not well confirmed experimentally. Furthermore, we have two higher spin resonances, $G_{17}(2190)$ and $H_{19}(2220)$, but we do not consider them in the present work because it is rather complicated to treat those higher spins unambiguously.

These two nucleon resonances can be established by the following effective Lagrangians:

$$\begin{aligned}
\mathcal{L}_{\gamma NN^*}\Big(\frac{3^\pm}{2}\Big) &= -\frac{ieh_1}{2M_N}\bar{N}\Gamma^{(\pm)}_\nu F^{\mu\nu}N^*_\mu \\
&\quad - \frac{eh_2}{(2M_N)^2}\partial_\nu\bar{N}\Gamma^{(\pm)}F^{\mu\nu}N^*_\mu + \text{H.c.}, \\
\mathcal{L}_{\gamma NN^*}\Big(\frac{5^\pm}{2}\Big) &= \frac{eh_1}{(2M_N)^2}\bar{N}\Gamma^{(\mp)}_\nu\partial^\alpha F^{\mu\nu}N^*_{\mu\alpha} \\
&\quad - \frac{ieh_2}{(2M_N)^3}\partial_\nu\bar{N}\Gamma^{(\mp)}\partial^\alpha F^{\mu\nu}N^*_{\mu\alpha} + \text{H.c.}, \quad (7)
\end{aligned}$$

where N^* stands for the field for the nucleon resonances with a certain spin and parity, and

$$\Gamma^{(\pm)}_\mu = \begin{pmatrix}\gamma_\mu\gamma_5\\ \gamma_\mu\end{pmatrix}, \qquad \Gamma^{(\pm)} = \begin{pmatrix}\gamma_5\\ \mathbf{1}\end{pmatrix}. \quad (8)$$

The coupling constants are determined by using the experimental data for the helicity amplitudes [15] and the quark model predictions of Ref. [21], which give $h_{1D_{13}} = 0.608(-0.770)$, $h_{2D_{13}} = -0.620(0.531)$, $h_{1D_{15}} = 0.123(-0.842)$, and $h_{2D_{15}} = 0.011(-0.782)$ for the proton (neutron). The effective Lagrangians for the relevant strong interactions are given as

$$\begin{aligned}
\mathcal{L}_{K^*N^*\Lambda}\Big(\frac{3^\pm}{2}\Big) &= -\frac{ig_{1D_{13}}}{2M_N}\bar{\Lambda}\Gamma^{(\pm)}_\nu K^{*\mu\nu}N^*_\mu - \frac{g_{2D_{13}}}{(2M_N)^2}\partial_\nu\bar{\Lambda}\Gamma^{(\pm)}K^{*\mu\nu}N^*_\mu + \frac{g_{3D_{13}}}{(2M_N)^2}\bar{\Lambda}\Gamma^{(\pm)}\partial_\nu K^{*\mu\nu}N^*_\mu + \text{H.c.}, \\
\mathcal{L}_{K^*N^*\Lambda}\Big(\frac{5^\pm}{2}\Big) &= \frac{g_{1D_{15}}}{(2M_N)^2}\bar{\Lambda}\Gamma^{(\mp)}_\nu\partial^\alpha K^{*\mu\nu}N^*_{\mu\alpha} - \frac{ig_{2D_{15}}}{(2M_N)^3}\partial_\nu\bar{\Lambda}\Gamma^{(\mp)}\partial^\alpha K^{*\mu\nu}N^*_{\mu\alpha} + \frac{ig_{3D_{15}}}{(2M_N)^3}\bar{\Lambda}\Gamma^{(\mp)}\partial^\alpha\partial_\nu K^{*\mu\nu}N^*_{\mu\alpha} + \text{H.c.}.
\end{aligned} \quad (9)$$

The corresponding scattering amplitudes can be obtained as

$$\begin{aligned}
\mathcal{M}_{s(N^*)}\Big(\frac{3^\pm}{2}\Big) &= \frac{1}{s-M^2_{N^*}}\epsilon^*_\nu\bar{u}_\Lambda\Big[\frac{g_1}{2M_N}\Gamma^{(\pm)}_\sigma + \frac{g_2}{(2M_N)^2}p_{2\sigma}\Gamma^{(\pm)} - \frac{g_3}{(2M_N)^2}k_{2\sigma}\Gamma^{(\pm)}\Big]\Delta_{\beta\alpha}(N^*,k_1+p_1) \\
&\quad\times\Big[\frac{eh_1}{2M_N}\Gamma^{(\pm)}_\delta \mp \frac{eh_2}{(2M_N)^2}\Gamma^{(\pm)}p_{1\delta}\Big](k_1^\alpha g^{\mu\delta} - k_1^\delta g^{\alpha\mu})u_N\epsilon_\mu \\
\mathcal{M}_{s(N^*)}\Big(\frac{5^\pm}{2}\Big) &= \frac{1}{s-M^2_{N^*}}\epsilon^*_\nu\bar{u}_\Lambda\Big[\frac{g_1}{(2M_N)^2}\Gamma^{(\mp)}_\delta + \frac{g_2}{(2M_N)^3}p_{2\delta}\Gamma^{(\mp)} - \frac{g_3}{(2M_N)^3}k_{2\delta}\Gamma^{(\mp)}\Big]k_2^\sigma(k_2^\rho g^{\nu\delta} - k_2^\delta\epsilon^{\nu\rho})\Delta_{\rho\sigma;\alpha\beta}(N^*,k_1+p_1) \\
&\quad\times\Big[\frac{eh_1}{(2M_N)^2}\Gamma^{(\mp)}_\lambda \pm \frac{eh_2}{(2M_N)^3}\Gamma^{(\mp)}p_{1\lambda}\Big]k_1^\beta(k_1^\alpha g^{\mu\lambda} - k_1^\lambda g^{\alpha\mu})u_N\epsilon_\mu,
\end{aligned} \quad (10)$$

TABLE III. Coupling constants for the resonances in Eqs. (9) and (11).

$h^p_{1D_{13}}$	$h^p_{2D_{13}}$	$h^p_{1D_{15}}$	$h^p_{2D_{15}}$	$h^n_{1D_{13}}$	$h^n_{2D_{13}}$	$h^n_{1D_{15}}$	$h^n_{2D_{15}}$	$g_{1D_{13}}$	$g_{2D_{13}}$	$g_{3D_{13}}$	$g_{1D_{15}}$	$g_{2D_{15}}$	$g_{3D_{15}}$
0.608	−0.620	0.123	0.011	−0.770	0.531	−0.842	−0.782	−1.59	0	0	1.03	0	0

where the spin-5/2 Rarita-Schwinger spin projection for the resonance R with momentum p is given by

$$\Delta_{\rho\sigma;\alpha\beta}(R,p) = (\not{p} + M_R)\Big[\frac{1}{2}(\bar{g}_{\rho\alpha}\bar{g}_{\sigma\beta} + \bar{g}_{\rho\beta}\bar{g}_{\sigma\alpha}) - \frac{1}{5}\bar{g}_{\rho\sigma}\bar{g}_{\alpha\beta} - \frac{1}{10}(\bar{\gamma}_\rho\bar{\gamma}_\alpha\bar{g}_{\sigma\beta} + \bar{\gamma}_\rho\bar{\gamma}_\beta\bar{g}_{\sigma\alpha} + \bar{\gamma}_\sigma\bar{\gamma}_\alpha\bar{g}_{\rho\beta} + \bar{\gamma}_\sigma\bar{\gamma}_\beta\bar{g}_{\rho\alpha})\Big]. \quad (11)$$

Here, we have used the following definitions of the *reduced* metric tensors and the gamma matrices:

$$\bar{g}_{\alpha\beta} = g_{\alpha\beta} - \frac{p_\alpha p_\beta}{M_R^2}, \qquad \bar{\gamma}_\alpha = \gamma_\alpha - \frac{p_\alpha}{M_R^2}\not{p}. \quad (12)$$

The strong coupling constants in Eq. (9) can be determined from the theoretical estimations for the partial-wave decay amplitudes,

$$\Gamma_{N^*\to K^*\Lambda} = \sum_\ell |G(\ell)|^2, \quad (13)$$

where $\Gamma_{N^*\to K^*\Lambda}$ is the decay width of $N^* \to K^*\Lambda$. The values for the partial-wave coupling strengths $G(\ell)$ can be found, e.g., in Ref. [22]. Since the purpose of the present work is to investigate the role of nucleon resonances near the threshold in the Born approximation, it must be a good approximation to take into account only the low partial-wave contributions. Hence, we consider only the g_1 terms in Eq. (9), employing only the lowest partial-wave contribution for $G(\ell)$. Then by using Eq. (13) and the prediction of Ref. [22], we obtain $|g_{1D_{13}}| = 1.59$ and $|g_{1D_{15}}| = 1.03$. The signs of these strong coupling constants are determined by fitting the experimental data. We list all the parameters of the resonances in Table III.

In the low-energy region we are interested in, the hadron cannot be simply viewed as a pointlike object but a spatially extended one, characterized by the phenomenological form factors in general. Hence, it is necessary to include the EM and hadronic form factors that represent the structure of hadrons probed by the photon and mesons, which violates gauge invariance of the amplitude. Thus, following the prescription described in Refs. [28–30], we write the reaction amplitudes as

$$\mathcal{M}_{\rm proton} = (\mathcal{M}_{K^*} + \mathcal{M}_p + \mathcal{M}_{\rm contact})F^2_{\rm common} + \mathcal{M}_K F_K^2 + \mathcal{M}_\kappa F_\kappa^2 + \mathcal{M}_\Lambda F_\Lambda^2 + \mathcal{M}_\Sigma F_\Sigma^2 + \mathcal{M}_{\Sigma^*}F^2_{\Sigma^*} + \mathcal{M}_{N^*}F^2_{N^*} \quad (14)$$

for $\gamma p \to K^{*+}\Lambda$ and

$$\mathcal{M}_{\rm neutron} = \mathcal{M}_K F_K^2 + \mathcal{M}_\kappa F_\kappa^2 + \mathcal{M}_n F_n^2 + \mathcal{M}_\Lambda F_\Lambda^2 + \mathcal{M}_\Sigma F_\Sigma^2 + \mathcal{M}_{\Sigma^*}F^2_{\Sigma^*} + \mathcal{M}_R F_R^2 \quad (15)$$

for $\gamma n \to K^{*0}\Lambda$. The form factors are defined generically as

$$F_{\rm common} = F_p F_{K*} - F_p - F_{K*}, \qquad F_\Phi = \frac{\Lambda_\Phi^2 - M_\Phi^2}{\Lambda_\Phi^2 - p^2}, \qquad F_B = \frac{\Lambda_B^4}{\Lambda_B^4 + (p^2 - M_B^2)^2}, \quad (16)$$

where p denotes the off-shell momentum of the relevant hadron. For the mesonic ($\Phi = K^*, K, \kappa$) and baryonic ($B = N, \Lambda, \Sigma, \Sigma^*, N^*$) vertices, we consider different types of the form factors with the cutoff parameters Λ_Φ and Λ_B. Those used in the present work are summarized in Table. IV, which are determined to reproduce the available cross section data for K^* photoproduction.

III. NUMERICAL RESULTS AND DISCUSSIONS

In this section, we present the results for various physical observables of charged and neutral $K^*\Lambda$ photoproduction. Shown in Fig. 2 are the differential cross sections of $\gamma p \to K^{*+}\Lambda$ for photon laboratory energies in the range of $E_\gamma = 2.15$ GeV − 2.65 GeV as functions of $\cos\theta$, where θ is the scattering angle of the K^* in the center-of-mass frame. Here, the dashed curves depict the cross sections of the background production mechanisms, and the contribution from the considered nucleon resonances (D_{13} and D_{15}) is given by the dotted-dashed curves. The solid ones draw their coherent sums. The obtained results are compared with the experimental data of the CLAS collaboration at TJNAF [3,19]. The present results show that the cross sections are enhanced in the forward direction because of the strong K-exchange contribution in the t channel. In the resonance region, i.e., $E_\gamma \approx 2$ GeV, the effects of the nucleon resonances are obvious but become smaller as

TABLE IV. Cutoff parameters in Eq. (16) for each channel.

Λ_{K*}	Λ_K	Λ_κ	Λ_N	Λ_Λ	Λ_Σ	Λ_{Σ^*}	$\Lambda_{D_{13}}$	$\Lambda_{D_{15}}$
0.9 GeV	1.25 GeV	1.25 GeV	0.9 GeV	0.9 GeV	0.9 GeV	0.9 GeV	1.2 GeV	1.2 GeV

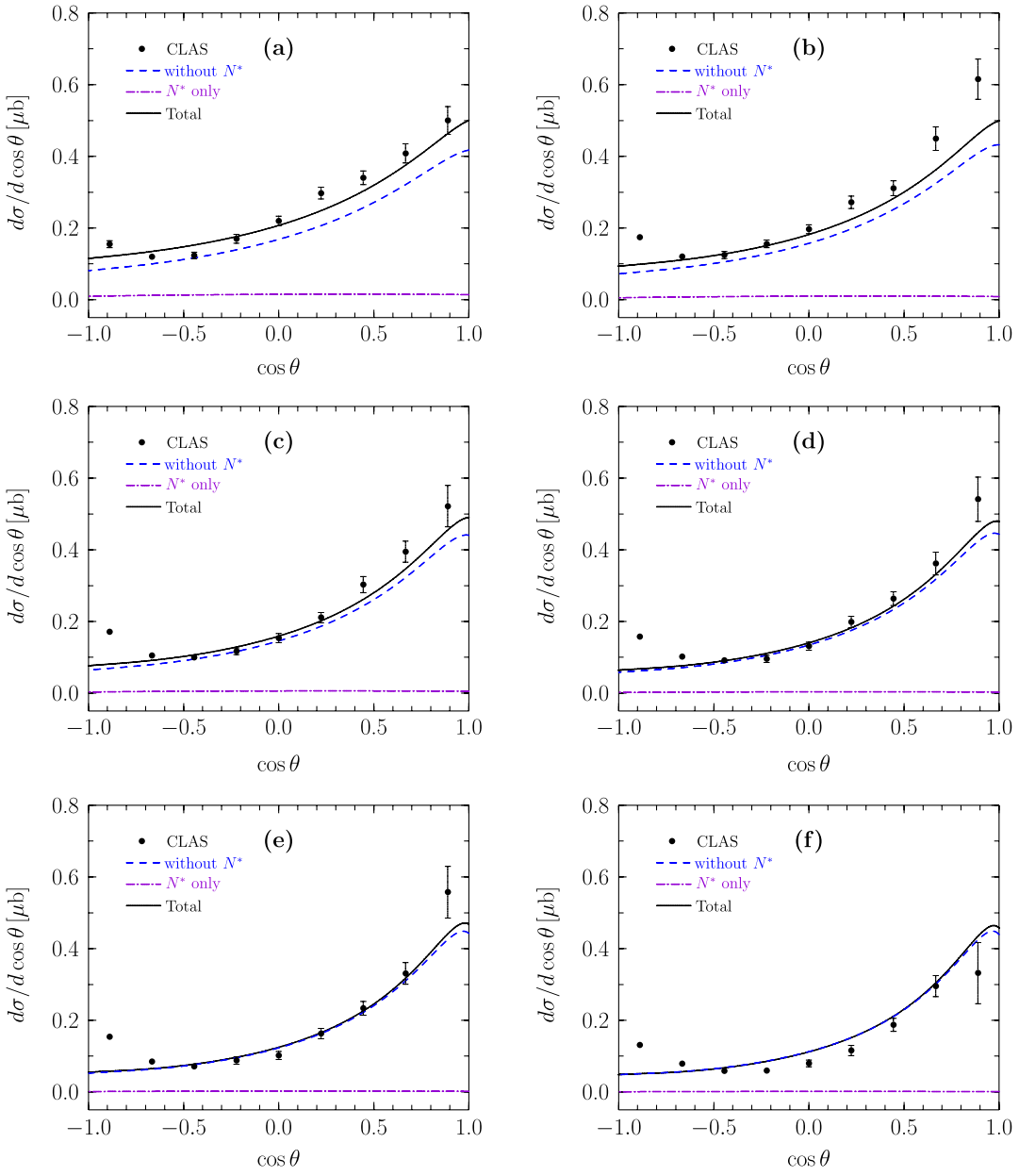

FIG. 2 (color online). Differential cross sections $d\sigma/\cos\theta$ for $\gamma p \to K^{*+}\Lambda$ at $E_\gamma =$ (a) 2.15 GeV, (b) 2.25 GeV, (c) 2.35 GeV, (d) 2.45 GeV, (e) 2.55 GeV, and (f) 2.65 GeV. Dashed curves explain the background production mechanisms whereas dotted-dashed ones are the contributions from nucleon resonances. The solid curve draws the total contribution from all relevant diagrams. The experimental data of the CLAS Collaboration are taken from Ref. [3].

the photon energy increases. Although our model can generally reproduce the cross section data qualitatively well, there is a discrepancy with the data in the backward scattering region. It implies nontrivial contributions from hyperon resonances in the u channel at large scattering angles. The role of hyperon resonances in K^* photoproduction will be reported elsewhere [31] (see, for example, Ref. [32].)

In Fig. 3, we show the obtained total cross section for $\gamma p \to K^{*+}\Lambda$ as a function of the photon laboratory energy E_γ. Since Ref. [3] does not report the total cross section data, we do not compare our results with the data.[3] The results of the total cross section exhibit a clear enhancement near the threshold. It implies that higher resonances appearing in this energy region play an essential role in explaining the mechanism of the $K^*\Lambda$ photoproduction. In particular, the contribution from the $D_{13}(2080)$ is prominent as shown by the dotted curve, while that of the

[3]We have not included the preliminary data for the total cross sections for $\gamma p \to K^{*+}\Lambda$ reported in Ref. [12] because of an error committed in the analyses [33].

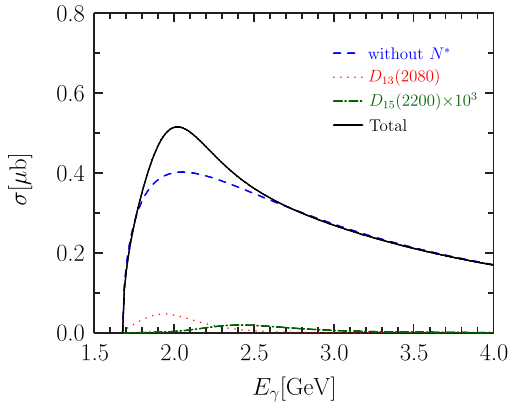

FIG. 3 (color online). Total cross sections for $\gamma p \to K^{*+}\Lambda$. The contributions from the $D_{13}(2080)$ and the $D_{15}(2200)$ are given by the dotted line and the dotted-dashed line, respectively. The dashed line is the result without nucleon resonances, and the solid line is the full calculation. Note that the D_{15} contribution is shown with factor 10^3 scaled.

$D_{15}(2200)$ (the dotted-dashed one) is almost negligible. In order to show how small the D_{15} contribution is, we have scaled it by factor 10^3. The dashed one depicts the background contribution, which is dominated by the K-meson exchange in the t channel. The contribution from the κ-meson exchange is small compared with that from the K-meson exchange, although it is larger than the other background diagrams near the threshold.

Using the same set of parameters, we can calculate the photon-beam asymmetry Σ_γ that is defined as

$$\Sigma_\gamma = \frac{d\sigma_\parallel - d\sigma_\perp}{d\sigma_\parallel + d\sigma_\perp}, \tag{17}$$

where $\parallel$ ($\perp$) indicates that the direction of the photon-polarization vector is parallel (perpendicular) to the reaction plane which is defined by the outgoing K^* momentum and the recoiled Λ momentum. In Fig. 4(a), the results of the asymmetry Σ_γ as a function of $\cos\theta$ at $E_\gamma = 2.25$ GeV are given, and those at $E_\gamma = 2.55$ GeV are drawn in Fig. 4(b). The dashed curves are the results without the nucleon resonances whereas the solid ones depict the results with all contributions. We immediately find that the asymmetry $\Sigma_\gamma \simeq 0$ without N^* contributions. Because of the strong magnetic-transition coupling of the nucleon resonances, however, the beam asymmetry Σ_γ turns negative with the N^* resonances included. Although the change is not drastically large, the size is noticeable enough to be tested by upcoming experimental measurements, in particular, at $\theta \simeq 0°$. This also can be seen in Fig. 5, where the asymmetry Σ_γ is given as a function of E_γ at scattering angle $\theta = 0°$, 60°, 90°, and 120°, respectively. As shown in Fig. 5(a), Σ_γ is almost compatible with zero for the whole energy region considered, though it increases mildly as E_γ increases. On the other hand, as the photon energy increases, the beam asymmetry becomes negative from the threshold, and its magnitude is getting increased up to around 2.2–2.4 GeV, depending on the scattering angle. Then it slowly decreases. Thus, it indicates that the N^* resonances are involved in changing the polarization of the K^* from the original spin alignment of the photon beam. We anticipate that the future experimental data will further clarify this point.

Figures 6–9 predict the observables of the $\gamma n \to K^{*0}\Lambda$ reaction. Shown in Fig. 6 is the total cross section for this reaction as a function of E_γ. Because of the neutral charge of the K^{*0}, the K^* exchange and the contact term are absent in this reaction as well as the electric photon-hyperon coupling. As in $\gamma p \to K^{*+}\Lambda$, the background production mechanisms are dominated by the K-meson exchange. However, since the neutral coupling of the $\gamma K K^*$ interaction is larger than that of the charged coupling by a factor of about $\sqrt{2}$, the total cross section for $\gamma n \to K^{*0}\Lambda$ turns out to be larger than those of $\gamma p \to K^{*+}\Lambda$ by a factor of 2.

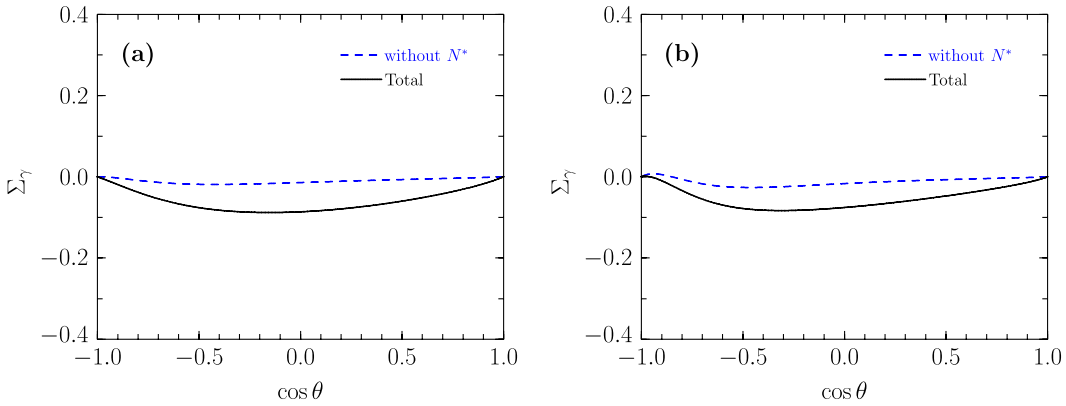

FIG. 4 (color online). Photon-beam asymmetry Σ_γ as a function of $\cos\theta$ for $\gamma p \to K^{*+}\Lambda$ at (a) $E_\gamma = 2.25$ GeV and (b) $E_\gamma = 2.55$ GeV.

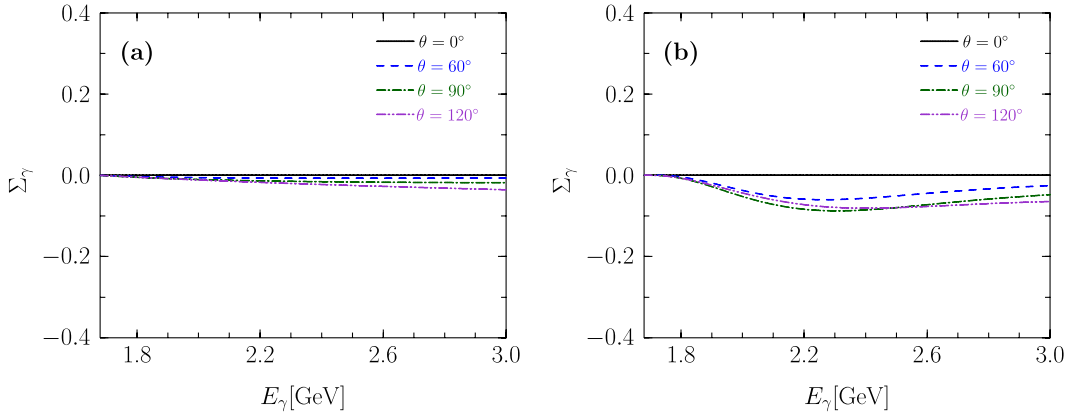

FIG. 5 (color online). Photon-beam asymmetry Σ_γ as a function of E_γ for $\gamma p \to K^{*+}\Lambda$ at $\theta = 0°$, 60°, 90°, and 120° (a) without the resonance contributions and (b) with the resonance contributions.

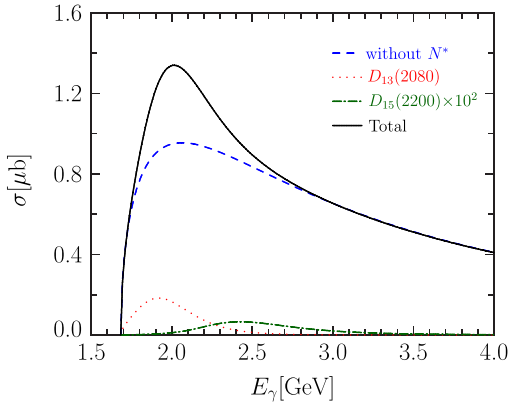

FIG. 6 (color online). Total cross sections for $\gamma n \to K^{*0}\Lambda$. The contributions from the $D_{13}(2080)$ and the $D_{15}(2200)$ are given by the dotted line and the dotted-dashed line, respectively. The dashed line is the result without nucleon resonances, and the solid line is the full calculation. Note that the D_{15} contribution is shown with factor 10^2 scaled.

As shown in Fig. 6, we again have considerable contributions from the D_{13} resonance near the threshold. Though the effect of the D_{15} on the neutron channel seems an order of magnitude larger than that on the proton channel, the contribution from the D_{15} remains negligible.

The differential cross sections for $\gamma n \to K^{*0}\Lambda$ are shown in Fig. 7 at $E_\gamma = 2.15$ GeV, 2.35 GeV, and 2.55 GeV, and the corresponding results are similar to those of $\gamma p \to K^{*+}\Lambda$. Unlike the charged K^* photoproduction, the differential cross sections slightly increase at the very backward scattering angle. We find that this behavior is caused by the interference among the u-channel contributions which depends on the isospin of the targets.

The results of the asymmetry Σ_γ are presented in Figs. 8 and 9. Figure 8 draws the angular distribution of Σ_γ at $E_\gamma = 2.25$ GeV and 2.55 GeV, whereas Fig. 9 shows the energy dependence of Σ_γ. The results are similar to those of $\gamma p \to K^{*+}\Lambda$. Namely, the contributions from the nucleon resonances change the asymmetry Σ_γ as in the case of the proton target.

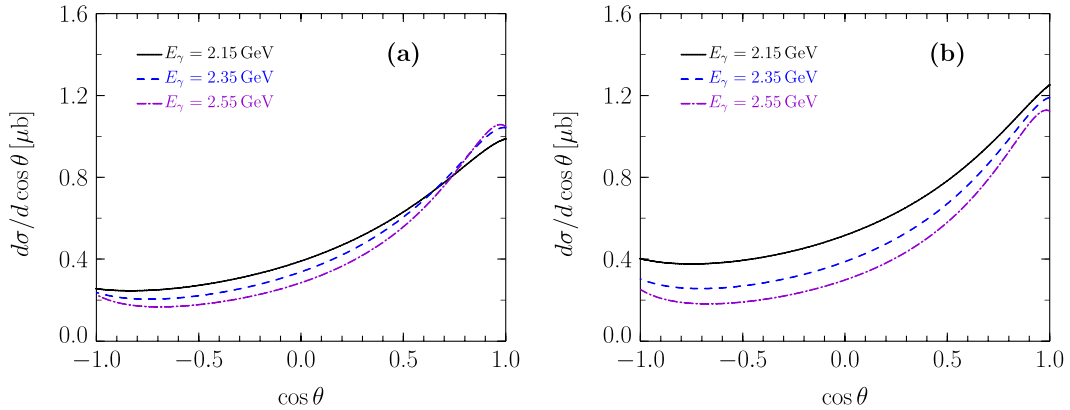

FIG. 7 (color online). Differential cross section $d\sigma/d\cos\theta$ for $\gamma n \to K^{*0}\Lambda$ at $E_\gamma = 2.15$ GeV, 2.35 GeV, and 2.55 GeV (a) without N^* contributions and (b) with N^* contributions.

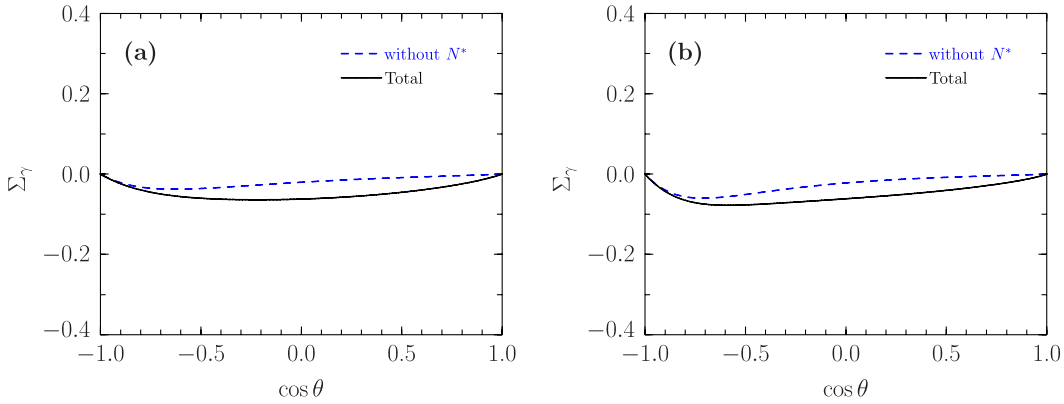

FIG. 8 (color online). Photon-beam asymmetry Σ_γ for $\gamma n \to K^{*0}\Lambda$ at (a) $E_\gamma = 2.25$ GeV and (b) $E_\gamma = 2.55$ GeV.

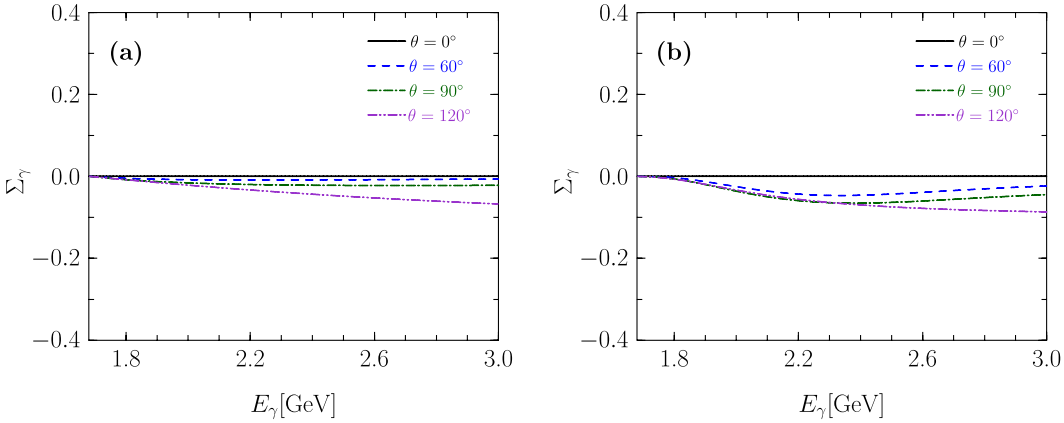

FIG. 9 (color online). Photon-beam asymmetry Σ_γ as a function of E_γ for $\gamma n \to K^{*0}\Lambda$ at $\theta = 0°, 60°, 90°$, and $120°$ (a) without the resonance contributions and (b) with the resonance contributions.

IV. SUMMARY AND CONCLUSION

In this work, we have studied $K^*\Lambda$ photoproduction off the nucleon target, i.e., $\gamma N \to K^*\Lambda$, focusing on the role of nucleon resonances, in particular, $D_{13}(2080)$ and $D_{15}(2200)$, the masses of which are close to the threshold of the reaction. We found that the recent differential cross section data of the CLAS Collaboration for the reaction of $\gamma p \to K^{*+}\Lambda$ were reasonably well-described by the present model except for the backward scattering region. It indicates that further investigations on the role of u-channel hyperon resonances are required [31]. The contributions from the nucleon resonances were found to be dominated by the $D_{13}(2080)$, and the D_{15} provides almost no corrections. The resonance parameters of the $D_{13}(2080)$ are determined by the experimental data of PDG [15] and the theoretical estimate of Ref. [21,22]. Although it requires more sophisticated analyses to precisely constrain the resonance parameters of the $D_{13}(2080)$, the present investigation shows that nucleon resonances contribute nontrivially to $K^*\Lambda$ photoproduction. It was also shown that the beam asymmetry was changed noticeably by the N^* resonances. The upcoming experimental data from the CLAS collaboration or from the LEPS collaboration will judge the role of these N^* resonances in K^* photoproduction.

The present model was also applied to the reaction of $\gamma n \to K^{*0}\Lambda$. We predicted the cross sections and the beam asymmetry of this reaction. We confirm that this reaction has larger cross sections than the $\gamma p \to K^{*+}\Lambda$ reaction, and the role of nucleon resonances is played in $\gamma n \to K^{*0}\Lambda$ as significantly as in $\gamma p \to K^{*+}\Lambda$. We expect that higher excited resonances of the nucleon may shed light on other photoproduction processes such as $\gamma N \to K^*\Sigma$. The corresponding investigation is under way.

ACKNOWLEDGMENTS

We are grateful to K. Hicks for kindly providing us with the experimental data and for constructive comments. We

also thank A. Hosaka and C. W. Kao for fruitful discussions. Two of us (S. H. K. and H. Ch. K.) were supported by Basic Science Research Program through the National Research Foundation of Korea funded by the Ministry of Education, Science and Technology (Grant No. 2009-0089525). The work of S. i. N. was partially supported by Grant No. NRF-2010-0013279 from the National Research Foundation of Korea. Y. O. was supported by the National Research Foundation of Korea Grant funded by the Korean Government (Grant No. NRF-2011-220-C00011).

[1] R. Bradford *et al.* (CLAS Collaboration), Phys. Rev. C **73**, 035202 (2006).
[2] P. Achenbach *et al.*, arXiv:1104.4245.
[3] K. Hicks, D. Keller, and W. Tang, AIP Conf. Proc. **1374**, 177 (2011).
[4] K. Tsukada *et al.*, Phys. Rev. C **78**, 014001 (2008).
[5] T. Watanabe *et al.*, Phys. Lett. B **651**, 269 (2007).
[6] S. Janssen, J. Ryckebusch, D. Debruyne, and T. Van Cauteren, Phys. Rev. C **65**, 015201 (2001).
[7] T. Mart, Phys. Rev. C **83**, 048203 (2011).
[8] B. G. Yu, T. K. Choi, and W. Kim, Phys. Lett. B **701**, 332 (2011).
[9] L. De Cruz, D. G. Ireland, P. Vancraeyveld, and J. Ryckebusch, Phys. Lett. B **694**, 33 (2010).
[10] T. Nakano (LEPS Collaboration), AIP Conf. Proc. **915**, 162 (2007).
[11] S. A. Pereira (CLAS Collaboration), Int. J. Mod. Phys. E **19**, 1021 (2010).
[12] L. Guo and D. P. Weygand (CLAS Collaboration), in International Workshop on the Physics of Excited Baryons NSTAR '05, Tallahassee, Florida, 2005 (to be published).
[13] I. Hleiqawi *et al.* (CLAS Collaboration), Phys. Rev. C **75**, 042201(R) (2007); **76**, 039905(E) (2007).
[14] M. Nanova *et al.* (CBELSA/TAPS Collaboration), Eur. Phys. J. A **35**, 333 (2008).
[15] K. Nakamura *et al.* (Particle Data Group), J. Phys. G **37**, 075021 (2010).
[16] Q. Zhao, J. S. Al-Khalili, and C. Bennhold, Phys. Rev. C **64**, 052201(R) (2001).
[17] Y. Oh and H. Kim, Phys. Rev. C **73**, 065202 (2006).
[18] Y. Oh and H. Kim, Phys. Rev. C **74**, 015208 (2006).
[19] K. Hicks, Baryons '10, Osaka, Japan (unpublished).
[20] S.-H. Kim, S. i. Nam, Y. Oh, and H.-Ch. Kim, AIP Conf. Proc. **1388**, 270 (2011).
[21] S. Capstick, Phys. Rev. D **46**, 2864 (1992).
[22] S. Capstick and W. Roberts, Phys. Rev. D **58**, 074011 (1998).
[23] D. Black, M. Harada, and J. Schechter, Phys. Rev. Lett. **88**, 181603 (2002).
[24] W. Rarita and J. Schwinger, Phys. Rev. **60**, 61 (1941).
[25] B. J. Read, Nucl. Phys. B **52**, 565 (1973).
[26] Th. A. Rijken, V. G. J. Stoks, and Y. Yamamoto, Phys. Rev. C **59**, 21 (1999).
[27] Y. Oh and H. Kim, Phys. Rev. D **70**, 094022 (2004).
[28] H. Haberzettl, C. Bennhold, T. Mart, and T. Feuster, Phys. Rev. C **58**, R40 (1998).
[29] R. M. Davidson and R. Workman, Phys. Rev. C **63**, 025210 (2001).
[30] H. Haberzettl, K. Nakayama, and S. Krewald, Phys. Rev. C **74**, 045202 (2006).
[31] S.-H. Kim, S. i. Nam, H.-Ch. Kim, and Y. Oh (unpublished).
[32] S. i. Nam and B.-G. Yu, arXiv:1109.3236.
[33] K. Hicks (private communication).